Computational and Theoretical Chemistry 1121 (2017) 1–10

Contents lists available at ScienceDirect

Computational and Theoretical Chemistry

journal homepage: www.elsevier.com/locate/comptc

Quantum chemical and kinetic study of the CCl_2 self-recombination reaction

Nicolás D. Gómez [a,*], Jorge Codnia [a], María L. Azcárate [a], Carlos J. Cobos [b,*]

[a] Departamento de Investigaciones en Láseres y Aplicaciones (CITEDEF- UNIDEF-CONICET), J. B. de La Salle 4397, (B1603ALO) Buenos Aires, Argentina
[b] Instituto de Investigaciones Fisicoquímicas Teóricas y Aplicadas (INIFTA), Departamento de Química, Facultad de Ciencias Exactas, Universidad Nacional de La Plata, CONICET, Casilla de Correo 16, Sucursal 4, (1900), Argentina

ARTICLE INFO

Article history:
Received 6 September 2017
Received in revised form 6 October 2017
Accepted 6 October 2017
Available online 7 October 2017

Keywords:
CCl_2
C_2Cl_4
Quantum-chemical calculations
Statistical adiabatic channel model/classical trajectory calculations
Recombination reactions

ABSTRACT

The temperature and pressure dependencies of the rate constant of the recombination reaction $CCl_2 + CCl_2 + M \rightarrow C_2Cl_4 + M$ have been theoretically studied between 300 and 2000 K. Quantum-chemical calculations were employed to characterize relevant parts of the potential energy surface of this process. The limiting rate constants were analyzed using the unimolecular reaction theory. The resulting low pressure rate constant can be represented as $k_0 = [Ar]\ 3.5 \times 10^{-23}\ (T/300\ K)^{-8.7}\ \exp(-1560\ K/T)\ cm^3\ molecule^{-1}\ s^{-1}$.

The high pressure rate constants derived from a simplified statistical adiabatic channel model (SSACM) and from a SACM combined with classical trajectory calculations (SACM/CT) are $k_\infty = (1.7 \pm 1.0) \times 10^{-12}\ (T/300)^{0.8 \pm 0.1}\ cm^3\ molecule^{-1}\ s^{-1}$ and $k_\infty = (5.4 \pm 3.0) \times 10^{-13}\ (T/300)^{0.7 \pm 0.1}\ cm^3\ molecule^{-1}\ s^{-1}$. The falloff curves were represented in terms of these limiting rate constants. Reported experimental results are satisfactorily described with the present model. The calculations indicate that the $CCl_2 + CCl_2$ reaction proceeds via the stabilization of C_2Cl_4, with a contribution of the $C_2Cl_3 + Cl \rightarrow C_2Cl_4$ reaction, and at sufficiently high temperatures the channel $CCl_2 + CCl_2 \rightarrow C_2Cl_2 + 2Cl$ becomes relevant.

1. Introduction

A large number of free radicals and metastable species can be generated via infrared multiphoton dissociation. Appreciable concentrations of these species are produced under low-pressure and short-time irradiation conditions, making the technique ideal for detailed kinetic studies.

The pyrolysis and photolysis of chloroform, $CHCl_3$, under a broad range of conditions has been extensively studied in the past few decades [1–17]. Reaction pathways to give account of the products determined at different stages of the reaction have been described. The three center HCl elimination reaction $CHCl_3 \rightarrow CCl_2 + HCl$ is the dominant initiation step [1,2,7,10,12–15]. The dominant pathway proposed to explain the formation of the main reaction product, C_2Cl_4, is the recombination reaction of two dichlorocarbene radicals, CCl_2 [1,2,14].

$$CCl_2 + CCl_2 + M \rightarrow C_2Cl_4 + M \quad (1)$$

This process has been scarcely studied. Won and Bozzelli [1] studied the pyrolysis of $CHCl_3$ in a reaction system consisting of 1% $CHCl_3$ in 760 Torr of Ar in the 800–1073 K temperature range. Gas chromatographic analysis was used to determine the concentrations of reactants and products as a function of temperature at different reaction times. They proposed a kinetic reaction mechanism consisting of 31 species and 67 elementary reactions to describe the reactant loss and the product formation. The rate constant for reaction (1) calculated using the unimolecular quantum version of the Rice-Ramsperger-Kassel (QRRK) theory was $1.1 \times 10^{-12}\ \exp(1300\ K/T)\ cm^3\ molecule^{-1}\ s^{-1}$. Kumaran et. al. [2] studied the pyrolysis of 1% and 4% $CHCl_3$ in Kr between 1282 and 1878 K. They used the laser schlieren technique to measure the $CHCl_3$ decomposition while the time resolved Cl formation was followed by the atomic resonance absorption spectroscopic technique. A reaction mechanism consisting of six elementary reactions was used to describe the secondary CCl_2 chemistry. To study the CCl_2 recombination reaction they carried out RRKM calculations on the dissociation of C_2Cl_4 to give $2CCl_2$. They estimated the equilibrium constant for $C_2Cl_4 \rightleftarrows 2\ CCl_2$ and calculated the third order recombination rate constant in the falloff region. The resulting values were fitted with the expression $1.6 \times 10^{-32}\ \exp(3000\ K/T)\ cm^6\ molecule^{-2}\ s^{-1}$. More recently, Zhu and Bozzelli [14] analyzed previous results of the

* Corresponding authors.
E-mail addresses: ndgomez@citedef.gob.ar (N.D. Gómez), cobos@inifta.unlp.edu.ar (C.J. Cobos).

https://doi.org/10.1016/j.comptc.2017.10.004
2210-271X/

thermal conversion of $CHCl_3$ to CCl_4 in the presence of Cl_2 over the 846–908 K temperature range using a detailed mechanism that included 38 elementary reactions. The QRRK rate constant for the CCl_2 self-recombination reported for a pressure of 0.1 atm over the 300–2000 K range was 3.0×10^{-5} (T/300 K)$^{-14.2}$ exp(−4600 K/*T*) cm^3 molecule^{-1} s^{-1}.

In previous works [16,17] we have experimentally determined the room temperature rate constant for reaction (1) using the laser induced fluorescence technique (LIF). In Ref. [16] The CCl_2 radicals were produced by infrared multiphoton dissociation (IRMPD) of 1 Torr of $CDCl_3$ in the presence of 0–30 Torr of Ar. The LIF technique allowed us to simplify the analysis of the reaction mechanism and determine the reaction rate constant in a direct manner. The value obtained for the rate constant at the high pressure limit was $k_\infty = (6.7 \pm 0.2) \times 10^{-13}$ cm^3 molecule^{-1} s^{-1}.

In the present work a theoretical study of the temperature and pressure dependencies of reaction (1) is reported. The relevant molecular properties were determined using density functional theory (DFT) and *ab initio* quantum-chemical calculations. Different approaches of the unimolecular reaction rate theory were employed to predict the rate constants.

2. Theoretical methods

The electronic structure calculations were carried out using the Gaussian 09 package [18]. The harmonic vibrational frequencies and rotational constants were determined with different approaches of the density functional theory. The standalone functional B97-D3 [19] and the following hybrid functionals B3LYP [20], B97-2 [21], B98 [22], mPW1PW91, mPW1LYP, mPW3PBE [23], TPSSh [24], B3PW91 [25–29], BH&HLYP, B3P86 [30], B1LYP [31–33], PBE1PBE [34,35], PBEh1PBE, X3LYP [36], B97-1 [37], APF, APF-D [38], mPW1PBE, LC-ωPBE [39–42], CAM-B3LYP [43] were combined with the MG3S basis set [44]. The basis set parameters were taken from Ref. [45]. This is a triple-zeta polarized basis set with diffuse functions on all heavy atoms which is equivalent to the Pople's 6-311+G(3d2f,2df,2p) basis set for H to Si atoms [46]. The reaction enthalpies and the electronic potential curves along the minimum energy pathways (MEP) were obtained from density functional theory and *ab initio* quantum-chemical calculations. The limiting high pressure rate constant was determined with a simplified version of the statistical adiabatic channel model, SSACM [47], and with the statistical adiabatic channel model/classical trajectory, SACM/CT, formulation developed for linear rotor + linear rotor type of reactions. [48]. The low pressure rate constants, k_0, were estimated using the strong collision low pressure rate coefficients, k_0^{SC}, obtained with a factorized model [49,50]. The pressure dependence of the rate constants in the intermediate falloff range were obtained with a recently formulated reduced falloff curves method [51,52].

3. Results

3.1. High pressure rate constant for $CCl_2 + CCl_2 \rightarrow C_2Cl_4$

The experimental study of Ref. [16] shows that reaction (1) is very close to the high pressure region. At the high pressure limit, radical recombination reactions and the reverse unimolecular bond fission process are dominated by the dynamics of the intramolecular process occurring above the reaction threshold energy. These type of reactions exhibit potential energy surfaces with a smooth transition between the reactants rotational modes and the specific vibrational motions of the formed molecule. In the frame of the SSACM the high pressure recombination rate constant is expressed as

$$k_\infty = f_{rigid}\ k_\infty^{pst} \tag{2}$$

Here k_∞^{pst} is the phase space theory rate constant which provides an upper bound to k_∞ and f_{rigid} is the so-called thermal rigidity factor that accounts for the contributions of the degrees of freedom orthogonal to the reaction coordinate, the transitional modes [53]. k_∞^{pst} depends on centrifugal contributions which are determined by the isotropic part of the potential and it is given by

$$k_\infty^{pst} = \frac{kT}{h}\left(\frac{h^2}{2\pi\mu kT}\right)^{3/2} f_{el} Q_{cent}^{*} \tag{3}$$

In this equation, μ denotes the reduced mass of the reaction partners and, for reaction (1), the electronic weight factor is $f_{el} = Q_{el}(C_2Cl_4)/Q_{el}(CCl_2)^2 = 1$. The evaluation of the centrifugal pseudo-partition function Q_{cent}^{*} requires the knowledge of the centrifugal barriers $E_0(J)$ (where J is the total angular momentum) which are obtained from the maxima of the expression $V(r, J) = D_0\{1 - exp[-\beta(r - r_e)]\}^2 + B_{cent}(r)\,J(J+1)$. The first term is a Morse potential with a range parameter β and equilibrium bond distance r_e. The second term takes into account the centrifugal potential, where the centrifugal constant $B_{cent}(r)$ varies along the MEP.

The centrifugal pseudo-partition function is approached with the expression,

$$Q_{cent}^{*} = \Gamma\left(1 + \frac{1}{\nu}\right)\left(\frac{kT}{C_\nu}\right)^{1/\nu}. \tag{4}$$

Here the centrifugal constants C_ν and ν are obtained from the centrifugal threshold pattern (see below).

For the present case, the effects of the potential anisotropy on k_∞ are accounted for in the rigidity factor,

$$f_{rigid} = \frac{(F_{AM}^{*}/\sigma^{*})\prod_{j=1}^{6} Q_j^{*}\prod_{m=1}^{6} Q_m^{*}}{Q_{vib}^2 Q_{rot}^2}\exp(-\Delta E_{0z}/kT) \tag{5}$$

In this expression, the pseudo-partition functions of the conserved and the transitional modes are denoted by Q_j^{*} and Q_m^{*}, respectively, Q_{rot} and Q_{vib} are the rotational and vibrational partition functions of CCl_2, respectively, σ^{*} is the effective symmetry number, and ΔE_{0z} is the adiabatic zero point barrier for the lowest reaction channel. The decoupling of J due to the factorization and separation of the loosening oscillators and rotors is corrected by the angular momentum coupling correction factor F_{AM}^{*}. The quantities denoted by *, as well ΔE_{0z}, depend on β and the looseness parameter α, defined as $\nu(r) = \nu_e \exp[-\alpha(r - r_e)]$, which account for the potential anisotropy. Here ν_e are the equilibrium vibrational frequencies of the transitional modes and r_e the C—C equilibrium bond distance in C_2Cl_4.

In a more recent formulation, the dynamics of the interaction between two linear rotors is treated as a combination of SACM and classical trajectory (CT) calculations. As in Ref. [47], a Morse potential and simple attenuation switching functions for the transitional modes are employed in this SACM/CT model [48]. For the present reaction, the CCl_2 radical was approached as a quasi-linear rotor with the C_{2v} symmetry axis assimilated to a $C_{\infty v}$ axis of a linear rotor, forming by association, a quasi-linear adduct C_2Cl_4. Then the rigidity factor at 0 K is given by

$$f_{\text{rigid}}(T \rightarrow 0) = (1 + 1.5Z + Z^4)^{-1/4} \tag{6}$$

where $Z = C_{eff}^2/2.34$ and $C_{eff} = \{[\varepsilon(r_e)]^2/2BD_e\}\ (kT/D_e)^{2\alpha/\beta-1}\ [1 + 0.4(2\alpha/\beta - 1) + (2\alpha/\beta - 1)^2]$. The geometrical average of the transitional frequencies at the equilibrium configuration is denoted by $\varepsilon(r_e)$ (see below), B is the average of the two lowest rotational constants of the CCl_2 radical and D_e is the Cl_2C—CCl_2 bond dissociation

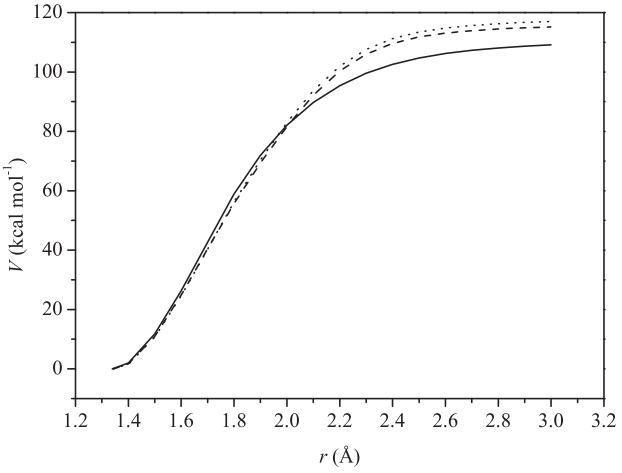

Fig. 1. Potential energy curve for $C_2Cl_4 \rightarrow CCl_2 + CCl_2$. (—): B3LYP/6-311+G(3*df*); (···): CBS-QB3; (–) G4.

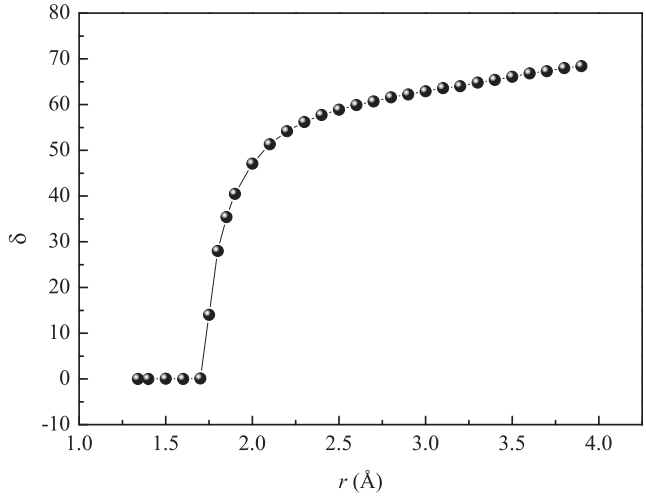

Fig. 3. Calculated δ angle (in degrees) along the MEP for $C_2Cl_4 \rightarrow CCl_2 + CCl_2$ at the B3LYP/6-311+G(3*df*) level.

energy. The computed $f_{rigid}(T \rightarrow 0)$ values were afterwards corrected by small temperature dependencies with the equation: $f_{rigid}(T) = f_{rigid}(T \rightarrow 0)\ [1 - (2.31C_{eff})\ (\beta r_e)^{1/2}\ \exp(X/2.044)]$ with $X = \ln(kT/D_e) - \beta\ r_{e,CM}$, being $r_{e,CM}$ the distance between the center of mass of CCl_2 radicals in C_2Cl_4.

In addition to structural and spectroscopic parameters of the molecular species, the calculation of k_∞ requires the knowledge of some features of the potential energy surface of the reaction. As abovementioned, the radial (isotropic) potential curve along the MEP is necessary for the prediction of k_∞^{PST}. The resulting curves calculated at the B3LYP/6-311+G(3*df*), CBS-QB3 [54] and G4 [55] levels of theory are depicted in Fig. 1. In the last two models, optimized structures at the B3LYP/6-311G(2*d*,*d*,*p*) (CBSB7 in the Gaussian 09 package) and B3LYP/6-31G(2*df*,*p*) levels are respectively employed.

As for the related reaction $CF_2 + CF_2 \rightarrow C_2F_4$ [56], Figs. 2 and 3 show a sharp departure from planarity when the C—C bond distance increases. In fact, as is seen in Fig. 3, the angle δ formed by the planes containing the CCl_2 radicals and the original plane of the C_2Cl_4 molecule increases abruptly from about 0° at ~1.5 Å to about 70° at large elongations. An animation is given in the electronic material illustrating this behavior.

On the other hand, if the C_2Cl_4 is forced to retain the planar structure, unrealistic potential curves with pronounced electronic barriers are obtained. This fact could be probably attributed to the π bond rupture when elongation increases.

The G4 model approaches the results obtained with the high-level *ab initio* method CCSD(T) combined with an extrapolated CBS basis set. Fig. 4 shows the G4 curve and the fit obtained for the high part of the potential using a Morse function with parameters $D_e = 117.0$ kcal mol^{-1}, $r_e = 1.344$ Å, and $\beta = 3.23$ Å^{-1}. As observed, a much better fit is clearly obtained with a Morse potential with an *r*-dependent β given by the equation $b_0 + b_1(r - r_e) + b_2(r - r_e)^2$.

However, similar k_∞^{pst} values of 3.76×10^{-10} and 3.19×10^{-10} cm^3 molecule^{-1} s^{-1}, and 9.59×10^{-10} and 8.24×10^{-10} cm^3 molecule^{-1} s^{-1} were obtained at 300 K and 2000 K with these curves, for the SSACM formalism. Therefore, the above standard potential with $\beta = 3.23$ Å^{-1} was used for all kinetic calculations. For comparison, potential curves computed at different DFT levels are included in Tables S1.1–S1.7 (see Supplementary Material). The parameters of the Morse potential are included in Table 1. It should be noted that the resulting average β value of (3.10 ± 0.28) Å^{-1} is in good agreement with the obtained with the G4 potential. On the other hand, the average DFT dissociation energy of (114 ± 6) kcal mol^{-1} is only 3 kcal mol^{-1} smaller than the predicted by the G4 model.

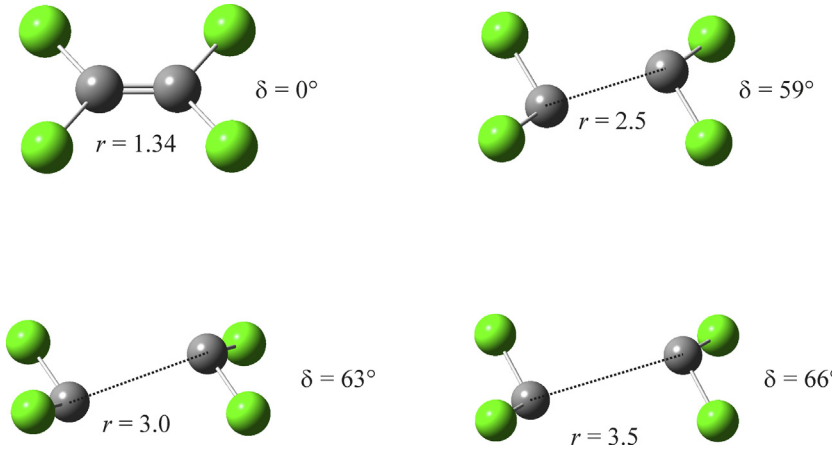

Fig. 2. C_2Cl_4 configurations computed along the MEP for $C_2Cl_4 \rightarrow CCl_2 + CCl_2$ at the B3LYP/6-311+G(3*df*) level.

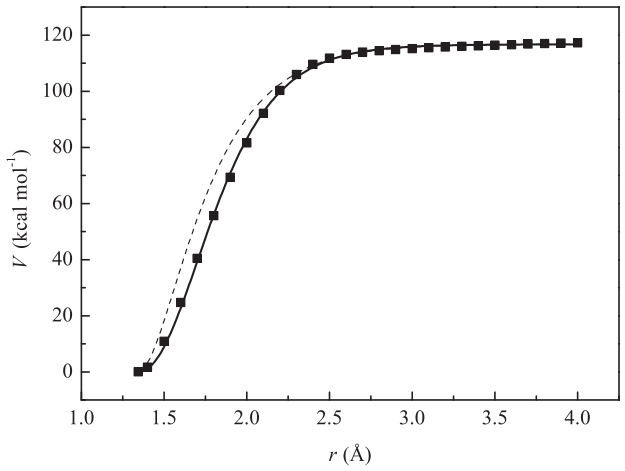

Fig. 4. Potential energy curve for $C_2Cl_4 \rightarrow CCl_2 + CCl_2$. (■): G4; (—): Morse potential with $\beta = 3.23$ Å^{-1}; (—): Morse potential with $\beta(r) = 1.88 + 1.77(r - 1.344) - 0.53(r - 1.344)^2$ Å^{-1}.

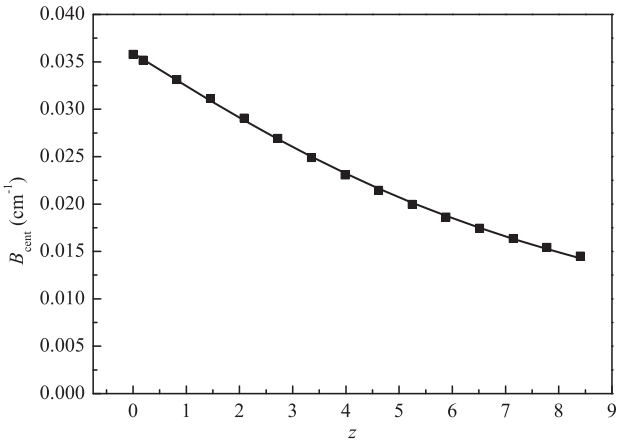

Fig. 5. Dependence of B_{cent} on $z = \beta(r - r_e)$ for $C_2Cl_4 \rightarrow CCl_2 + CCl_2$ calculated at the B3LYP/MG3S level. For the results of the fit see the text.

Table 1
Morse parameters for the dissociation reaction $C_2Cl_4 \rightarrow CCl_2 + CCl_2$ for different DFT levels.

Level of theory	D_e/kcal mol^{-1}	β/Å^{-1}
B3LYP	110	3.16
B97-2	113	3.21
B98	110	3.10
mPW1PW91	118	3.11
PBEPBE	112	2.65
TPSSh	110	2.93
BLYP	101	2.85
PBELYP	104	2.70
B97-D3	106	2.63
B3PW91	116	3.10
BH&HLYP	116	3.70
B3P86	118	2.96
B1LYP	109	3.29
mPW1LYP	110	3.29
mPW3PBE	117	3.03
PBE1PBE	120	3.03
PBEh1PBE	119	3.05
X3LYP	111	3.20
B97-1	110	3.09
APF	118	3.06
APF-D	119	2.88
mPW1PBE	118	3.11
LC-ωPBE	126	3.77
CAM-B3LYP	117	3.42

As abovementioned, to calculate Q^*_{cent}, the rotational constants $B_{cent}(r)$ along the MEP and the parameters C_ν and ν are required. The computed $B_{cent}(r)$ values at the B3LYP/MG3S level are depicted in Fig. 5. A fit using the expression $B_{cent}(r) = B_e/[1 + a_1 z + a_2 z^2]$ with $z = \beta(r - r_e)$ [47], leads to the parameters $B_e = 3.59 \times 10^{-2}$ cm^{-1}, $a_1 = 9.76 \times 10^{-2}$ and $a_2 = 9.88 \times 10^{-3}$.

The C_ν and ν values were obtained from the $E_0(J) - E_0(J = 0) \approx C_\nu [J(J + 1)]^\nu$ relationship (Fig. 6), where the $E_0(J)$ values are calculated from the maxima of the above given centrifugal potential $V(r, J)$. The B_e, a_1, a_2, C_ν and ν values derived from different DFT models are listed in Table S2.1 of the Supplementary Material.

To evaluate f_{rigid} the correlation scheme of the transitional modes must be characterized. In the SSACM (Eq. (5)), the number of disappearing oscillators (including the K rotor), which correlate with the two CCl_2 rotors, is equal to six. The corresponding correlation scheme is: $C(C_2Cl_4) \leftarrow \varepsilon_K \rightarrow A(CCl_2)$ (m = 1), $\nu_{twist} \leftarrow \varepsilon_{twist} \rightarrow A(CCl_2)$ (m = 2), $\nu_{s-rock} \leftarrow \varepsilon_{s-rock} \rightarrow B(CCl_2)$ (m = 3), $\nu_{s-wagg} \leftarrow \varepsilon_{s-wagg} \rightarrow B(CCl_2)$ (m = 4), $\nu_{a-rock} \leftarrow \varepsilon_{a-rock} \rightarrow C(CCl_2)$ (m = 5) and

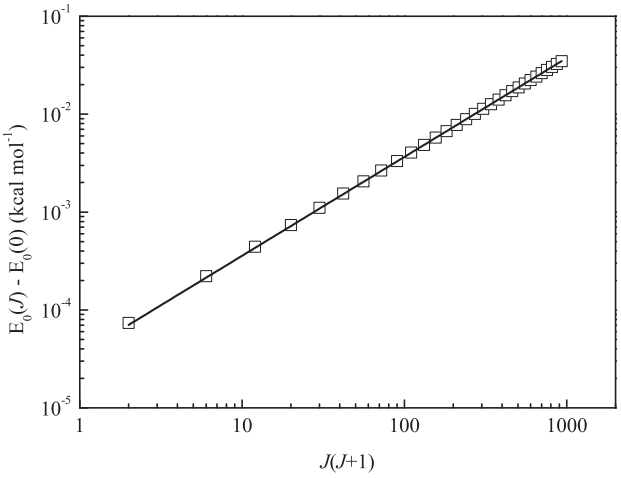

Fig. 6. Centrifugal barrier dependence on $J(J + 1)$. Calculations performed at the B3LYP/MG3S level.

$\nu_{a-wagg} \leftarrow \varepsilon_{a-wagg} \rightarrow C(CCl_2)$ (m = 6). The mode denoted by ν_{twist} = 110 cm^{-1} corresponds to the CCl_2 twist motion, ν_{s-rock} = 176 cm^{-1} and ν_{a-rock} = 347 cm^{-1} are the symmetric and antisymmetric rocking modes, and ν_{s-wagg} = 288 cm^{-1} and ν_{a-wagg} = 512 cm^{-1} are the symmetric and antisymmetric wagging modes. In the SSACM, the evolution of these specific vibrational modes along the MEP is accounted for by the above defined α looseness parameter. As Fig. 7 shows, a linear logarithmic decay of $\nu_i(r)$ is observed for the disappearing oscillators computed at the B3LYP/MG3S level.

A similar behavior has been observed for the other DFT methods employed. The resulting α values are given in Table 2.

As Table 3 shows, the average of the derived individual α parameters in Table 2 is (1.28 ± 0.21) Å^{-1} (with 3σ significance), i.e., comparable with the value obtained from a large number of experimental recombination reactions, (1.06 ± 0.30) Å^{-1} [53].

Besides, the resulting average ratio $\alpha/\beta = 1.28$ Å$^{-1}/3.23$ Å^{-1} = 0.40 is in reasonable agreement with the obtained in Ref. [53] of (0.46 ± 0.09).

Using the individual α parameters, $\beta = 3.23$ Å^{-1}, $\nu \approx 1.01$, and $C_\nu \approx 0.012$, SSACM values for k^{pst}_∞, f_{rigid} and k_∞ for each DFT model employed were derived. Results for k_∞ and f_{rigid} are given in Tables S3.3 and S3.4 of the Supplementary Material. The average values

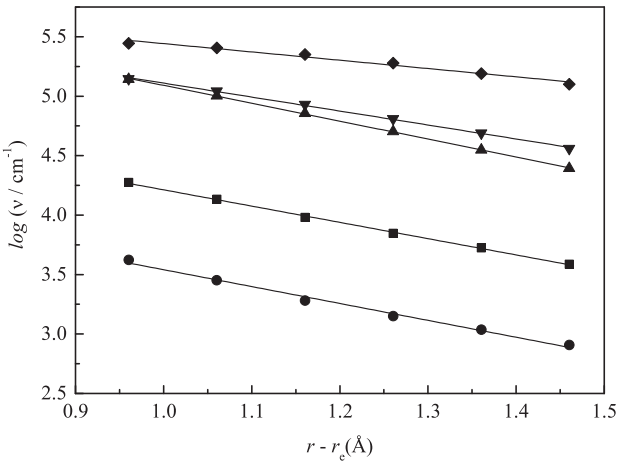

Fig. 7. B3LYP/MG3S harmonic transitional frequencies along the MEP for $C_2Cl_4 \rightarrow CCl_2 + CCl_2$. (■): twist ($\alpha = 1.37$ Å^{-1}); (●): s-rock ($\alpha = 1.42$ Å^{-1}); (▲): a-rock ($\alpha = 1.51$ Å^{-1}); (▼): s-wagg ($\alpha = 1.17$ Å^{-1}) (◆): a-wagg ($\alpha = 0.70$ Å^{-1}).

Table 2
α Values (in Å^{-1}) for the different transitional modes calculated at different levels of theory.

Level of theory	CCl_2 twist	CCl_2 s-rock	CCl_2 a-rock	CCl_2 s-wagg	CCl_2 a-wagg
BH&HLYP	1.49	1.35	1.63	1.24	0.55
B98	1.39	1.13	1.54	1.21	0.82
B97-2	1.35	1.46	1.54	1.22	0.82
mPW1LYP	1.41	1.35	1.56	1.24	0.76
X3LYP	1.39	1.37	1.54	1.22	0.79
mPW1PBE	1.48	1.29	1.57	1.28	0.87
B1LYP	1.35	1.32	1.55	1.21	0.71
PBELYP	1.25	1.70	1.37	1.07	0.87
mPW3PBE	1.45	1.31	1.53	1.23	0.93
PBEPBE	1.37	1.63	1.38	1.10	0.91
B97-D3	1.27	2.03	1.37	1.17	1.21
mPW1PW91	1.48	1.30	1.57	1.28	0.87
TPSSh	1.59	1.66	1.48	1.30	0.95
B97-1	1.37	1.03	1.53	1.16	0.85
B3PW91	1.42	1.33	1.54	1.24	0.84
BLYP	1.17	1.40	1.37	1.08	0.76
B3LYP	1.37	1.42	1.51	1.17	0.70
B3P86	1.43	1.38	1.54	1.26	0.90
PBE1PBE	1.50	1.34	1.57	1.24	0.92
PBEh1PBE	1.51	1.47	1.56	1.23	0.92
APF	1.46	1.32	1.55	1.23	0.91
APF-D	1.48	1.69	1.56	1.19	1.26
LC-ωPBE	1.34	1.02	1.61	1.19	0.71
CAM-B3LYP	1.50	1.34	1.62	1.21	0.75

derived from these kinetics' data are given in Table 4. The deviation between the k_∞ values computed with the different DFT models, relative to the mean value, and over the 300–2000 K range is ≈30–50%.

For the SACM/CT calculations, for each DFT model, the average of the α values corresponding to the different transitional modes (Table 3) was employed. The deviation between the k_∞ values obtained with the different DFT models, relative to the mean value, and over the 300–2000 K range is ≈30–50%. The average values derived from these kinetic data are given in Table 5 and detailed data can be found in Tables S3.5 and S3.6 of the Supplementary Material.

k_∞ values calculated with SSACM are a factor of 3 higher than the ones calculated with the SACM/CT formulation developed for linear rotor + linear rotor addition. The predicted temperature dependence for the SSACM and SACM/CT rate coefficients are $k_\infty = (1.7 \pm 1.0) \times 10^{-12}\,(T/300)^{0.8 \pm 0.1}$ cm^3 molecule^{-1} s^{-1} and $k_\infty = (5.4 \pm 3.0) \times 10^{-13}\,(T/300)^{0.7 \pm 0.1}$ cm^3 molecule^{-1} s^{-1}, respectively. The uncertainties in the fitted parameters are estimated as 1σ of the results obtained for the different functionals employed. On one hand, the variations in the values calculated for k_∞^{pst} are due to differences in the calculation of the centrifugal energy. As previously described in the SACM/CT model, the interaction of two linear species forming a quasi-linear adduct is considered. In the SSACM the centrifugal potential is approximated with that of a symmetric top molecule and Q^*_{cent} is calculated considering a quasi-diatomic or quasi-triatomic centrifugal potential for the adduct, described by the mean value of the two smallest rotational constants. On the other hand, rigidity factors calculated in the SSACM formalism differ from those calculated by SACM/CT in that the coupling between the angular momentum and the conserved and disappearing oscillators is neglected in SACM/CT. The difference between the values obtained for these factor with both formalisms is within 40%.

Table 3
Average α values obtained from all DFT methods.

Level of theory	α/Å^{-1}	Level of theory	α/Å^{-1}
BH&HLYP	1.25	TPSSh	1.40
B98	1.22	B97-1	1.19
B97-2	1.28	B3PW91	1.27
mPW1LYP	1.26	BLYP	1.16
X3LYP	1.26	B3LYP	1.23
mPW1PBE	1.30	B3P86	1.30
B1LYP	1.23	PBE1PBE	1.31
PBELYP	1.25	PBEh1PBE	1.34
mPW3PBE	1.31	APF	1.29
PBEPBE	1.28	APF-D	1.44
B97-D3	1.41	LC-ωPBE	1.17
mPW1PW91	1.30	CAM-B3LYP	1.28

Table 4
Average values for the SSACM high pressure rate coefficients k_∞^{pst} and k_∞ (in cm^3 molecule^{-1} s^{-1}) and the rigidity factors f_{rigid} for $CCl_2 + CCl_2 \rightarrow C_2Cl_4$ calculated with the α values of Table 2 and $\beta = 3.23$ Å^{-1}.

T (K)	k_∞^{pst}	f_{rigid}	k_∞
300	3.76×10^{-10}	3.51×10^{-3}	1.33×10^{-12}
500	4.84×10^{-10}	4.87×10^{-3}	2.38×10^{-12}
1000	6.81×10^{-10}	6.59×10^{-3}	4.51×10^{-12}
1500	8.32×10^{-10}	7.22×10^{-3}	6.04×10^{-12}
2000	9.59×10^{-10}	7.36×10^{-3}	7.10×10^{-12}

Table 5
SACM/CT high pressure rate coefficients k_∞^{pst} and k_∞ (in cm^3 molecule^{-1} s^{-1}) and rigidity factors f_{rigid} for $CCl_2 + CCl_2 \rightarrow C_2Cl_4$ calculated with the α values of Table 3.

T (K)	k_∞^{pst}	f_{rigid}	k_∞
300	1.93×10^{-10}	2.75×10^{-3}	5.31×10^{-13}
500	2.34×10^{-10}	3.24×10^{-3}	7.60×10^{-13}
1000	3.04×10^{-10}	4.03×10^{-3}	1.23×10^{-12}
1500	3.54×10^{-10}	4.55×10^{-3}	1.61×10^{-12}
2000	3.94×10^{-10}	4.95×10^{-3}	1.95×10^{-12}

In a previous work we determined $k_\infty = (6.7 \pm 0.2) \times 10^{-13}$ cm^3 molecule^{-1} s^{-1} by extrapolation of the measured second-order rate coefficients over the 0–30 Torr of Ar range (1 Torr of $CDCl_3$) with a simple Lindemann-Hinshelwood expression. Within theoretical and experimental uncertainties, both SSACM and SACM/CT room temperature values are in good agreement with the experimental result.

3.2. Low pressure rate constant for $CCl_2 + CCl_2 \rightarrow C_2Cl_4$

In addition to the intramolecular dynamics inherent to the limiting high pressure rate coefficients, the recombination reactions in

Table 6
Contributing factors to k_0 for $CCl_2 + CCl_2 + Ar \rightarrow C_2Cl_4 + Ar$. Z_{LJ} in cm^3 $molecule^{-1}$ s^{-1}, k_0/[M] in cm^6 $molecule^{-2}$ s^{-1} and K_C in molecule cm^{-3}.

T/K	Z_{LJ}	Q_{vib}	F_E	F_{rot}	β_c	K_C	k_0/[M]
300	4.13×10^{-10}	17.29	1.06	7.46	0.24	8.2×10^{-55}	2.21×10^{-25}
500	4.53×10^{-10}	205.20	1.10	5.46	0.16	1.01×10^{-24}	1.76×10^{-26}
1000	5.32×10^{-10}	2.6×10^{4}	1.21	3.44	0.085	3.92×10^{3}	2.17×10^{-28}
1500	5.93×10^{-10}	8.9×10^{5}	1.35	2.58	0.055	4.00×10^{11}	1.06×10^{-29}
2000	6.43×10^{-10}	1.4×10^{7}	1.51	2.09	0.039	3.20×10^{15}	1.08×10^{-30}

the intermediate falloff region depend also on specific intermolecular processes assisted by molecular collisions. At the low pressure limit, these last processes are predominant and taken into account by the low pressure rate coefficient k_0. A convenient and frequently employed approach to estimate k_0 is provided by the Troe's factorized formalism: $k_0 = \beta_c\ k_0^{SC}$ [49,50]. Here, the strong-collision rate coefficient, k_0^{SC}, is characterized by the equilibrium population of molecular states, and the collision efficiency, β_c, depends on intermolecular energy transfer processes. k_0^{SC} is given by,

$$k_0^{SC} = (1/K_C)[M]\,Z_{LJ}\,\frac{\rho_{vib,h}(E_0)kT}{Q_{vib}(C_2Cl_4)}\exp\left(-\frac{E_0}{kT}\right)F_{anh}\,F_E\,F_{rot}\,F_{rotint} \quad (7)$$

In this expression, Z_{LJ} is the collision frequency between the excited adduct and the bath gas M; E_0 is the threshold or dissociation energy, given by the reaction enthalpy $\Delta_R H^0$ at 0 K; $\rho_{vib,h}(E_0)$ is the harmonic vibrational density of states evaluated at E_0; F_E takes into consideration the energy dependence of $\rho_{vib,h}(E_0)$; F_{anh} accounts for anharmonicity; F_{rot} for the rotational effects on state densities; F_{rotint} describes the internal rotor behavior (almost 1 for the present reaction); $Q_{vib}(C_2Cl_4)$ is the vibrational partition function of the dissociated molecule and K_C is the equilibrium constant estimated, as usual, from the molecular partition functions. For $\rho_{vib,h}(E_0)$ and F_{anh} the values $2.31 \times 10^{14}\,(kcal\ mol^{-1})^{-1}$ and 1.75 were respectively employed. The expressions for the respective correction factors are given in Ref. [49,50]. Calculated factors and resulting k_0 values are listed in Table 6 and Table S4.1 (see Supplementary Material)).

The resulting strong collision rate constant can be represented between 300 and 2000 K by the equation

$$k_0^{SC} = [Ar]7.2\ x\ 10^{-23}(T/300\ K)^{-7.4}\exp(-1330\ K/T)\ cm^3\ molecule^{-1}\ s^{-1} \quad (8)$$

And the equilibrium constant is given by the expression,

$$K_c = 5.6\ x\ 10^{29}(T/300\ K)^{-1.9}\ \exp(58000\ K/T)\ molecule\ cm^{-3} \quad (9)$$

The limiting low pressure rate coefficient including weak collision effects resulted in,

$$k_0 = [Ar]3.5\ x\ 10^{-23}(T/300\ K)^{-8.7}\ \exp(-1560\ K/T)\ cm^3\ molecule^{-1}\ s^{-1} \quad (10)$$

The β_c values were derived from the expression [50]

$$-\langle\Delta E\rangle \approx F_E\ kT\ \beta_c/(1-\beta_c^{1/2}) \quad (11)$$

with a temperature independent average energy transferred in up and down C_2Cl_4 - Ar collisions of $-\langle\Delta E\rangle \approx 100\ cm^{-1}$. This value is found to be in good agreement with previously reported values for large polyatomic molecules over wide ranges of vibrational excitation [57]. The temperature dependence is generally found to be small for most cases, and almost negligible for noble gases.

Evaluation of k_0^{SC} and K_c requires knowledge of E_0. In the present work this parameter was calculated with the G4 method, obtaining 114 kcal mol^{-1}. There is certain uncertainty in the values reported in the literature for $\Delta_f H^0(CCl_2)$ and $\Delta_f H^0(C_2Cl_4)$. The values reported in the NIST-JANAF [58] thermochemical database tables are $\Delta_f H^0(CCl_2) = 56.96$ kcal mol^{-1}, and $\Delta_f H^0(C_2Cl_4) = -2.85$ kcal mol^{-1}, respectively, resulting in $E_0 = 117$ kcal mol^{-1}. The values of the thermochemical database for combustion reported by Burcat and Ruscic [59] are $\Delta_f H^0(CCl_2) = 55.32$ kcal mol^{-1} and $\Delta_f H^0(C_2Cl_4) = -5.60$ kcal mol^{-1}, thus, the calculated dissociation energy is $E_0 = 116$ kcal mol^{-1}. Demaison et al. [60] studied the thermochemistry of CF_2 and CCl_2 radicals and calculated the heats of formation at 0 K using W2 method, reporting $\Delta_f H^0(CCl_2) = 54.48$ kcal mol^{-1}. The heats of formation at 0 K for CF_2, CCl_2 and CBr_2 radicals were computed by Sendt et al. [61] employing the CCSD(T) method in the complete basis set limit. The results obtained for CCl_2 are similar to those reported by Demaison et al. Combining the $\Delta_f H^0(C_2Cl_4)$ values reported in the NIST-JANAF and Burcat et al. tables with those of $\Delta_f H^0(CCl_2)$ reported by Demaison et al. leads to dissociation energies of 112 kcal mol^{-1} and 115 kcal mol^{-1}, respecteively. Taking into account the dispersion of the enthalpy of reaction values of the CCl_2 self-recombination reaction, the uncertainty of the E_0 value can be estimated in 2 kcal mol^{-1}. This uncertainty in E_0 leads to an uncertainty in k_0^{sc} of 20% and of ± 4 cm^{-1} in $-\langle\Delta E\rangle$.

3.3. Rate coefficients in the falloff range

The transition of the recombination rate constants from the low to the high pressure range was carried out with the following falloff expression [52]:

$$k/k_\infty = F_{LH}(x)\,F(x) \quad (12)$$

where $x = k_0/k_\infty$, $F_{LH}(x)$ is the Lindemann-Hinshelwood factor defined as

$$F_{LH}(x) = x/(1+x) \quad (13)$$

and $F(x)$ the broadening factor given by

$$F(x) = \frac{1+x}{[1+x^n]^{1/n}} \quad (14)$$

with

$$n = \left[\frac{ln(2)}{ln(2/F_{cent})}\right][1 - 0.15\,(1-x^q)] \quad (15)$$

$$q = (F_{cent}-1)/ln(F_{cent}/10) \quad (16)$$

The essential magnitude in the broadening factor $F(x)$ is the center broadening factor, F_{cent}. Eqs. (14)–(16) reproduce very well the asymmetric broadening factors for broad falloff curves, as characterized by values of the center broadening factors F_{cent} below ≈0.4. Previously proposed expressions for $F(x)$ work equally well for $F_{cent} > 0.4$. The expressions of Eqs. (13)–(15) allow for the representation of falloff curves over much larger ranges of F_{cent}, covering all cases of practical need. A description of the determination of F_{cent} and $F(x)$ is given in Section 5 of the Supplementary Material. Over the 300–2000 K temperature range F_{cent} varies between 0.2 and 0.04. An appropriate representation of F_{cent} including weak collision effects is given by

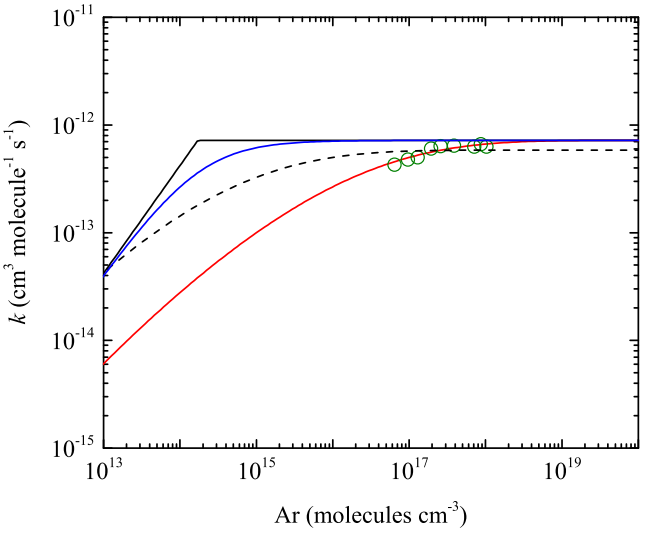

Fig. 8. Falloff curve for $CCl_2 + CCl_2 + Ar \rightarrow C_2Cl_4 + Ar$. Experiment (Ref. [16]), Q. Fitting parameters $-\langle\Delta E\rangle = 60\ cm^{-1}$, $T = 600\ K$ and $k_\infty = 7.2 \times 10^{-13}\ cm^3\ molecule^{-1}\ s^{-1}$, (Red line). Eq. (12) with $F(x) = 1$, (Blue line). Fitting with T = 300 K (Dashed black line). (For interpretation of the references to colour in this figure legend, the reader is referred to the web version of this article.)

$$F_{cent}(Ar) = \exp(-T/1800\ K) + 0.88[\exp(-T/170\ K) - \exp(-T/1800\ K)] + \exp(-8100\ K/T) \quad (17)$$

Experimental results for the rate coefficients of the self-recombination reaction of CCl_2 radicals of Ref. [16] were fitted with expressions (12)–(16), employing $-\langle\Delta E\rangle$, T and k_∞ as fitting parameters. k_∞ was allowed to vary within 2σ of the theoretical values resultant from SSACM and SACM/CT calculations. Theoretical results are consistent with experimental values provided T is in the 500–700 K range, $-\langle\Delta E\rangle$ within 10 cm^{-1} and 250 cm^{-1} and $k_\infty = (7.2 \pm 0.4) \times 10^{-13}\ cm^3$ molecules^{-1} s^{-1}. We may also fit the experimental falloff curve with the widely used simple symmetric broadening factor, $F_{cent}^{\{1/[1+(\log(x/N))^2]\}}$ with $N = 0.75-1.27\log(F_{cent})$ [62]. Within experimental and theoretical scatter, this equation provides satisfactory representations of the experimental falloff curve, obtaining similar results as those using Eqs. (14)–(16). Fig. 8 shows the experimental results obtained in Ref. [16] for Ar pressures in the 1–30 Torr range, and the results of the calculations with $-\langle\Delta E\rangle = 60\ cm^{-1}$, $T = 600\ K$ and $k_\infty = 7.2 \times 10^{-13}\ cm^3$ molecules^{-1} s^{-1}. By contrast to this very good fit, a modeling using T = 300 K strongly overestimates the experimental falloff curve.

Regarding temperature effects, intermolecular energy transfer is of great interest for understanding fundamental pyrolysis reactions and laser induced chemistry. Oref and Tardy [57] and Hippler and Troe [63] reviewed the collisional energy transfer in highly excited polyatomic molecules. Energy transfer in small molecules at low levels of excitation was reviewed by Flynn [64]. The range of $-\langle\Delta E\rangle$ values found in the present work is consistent with that of other systems at different excitation and temperature conditions. The high uncertainty in $-\langle\Delta E\rangle$ is due to the correlation between T and β_c as expressed in Eq. (11) and the dependence of k_0^{sc} on T as described in Eq. (8).

The range of temperatures found in the fitting can be interpreted in terms of the energy relaxation of the CCl_2 radicals obtained in the dissociation of $CDCl_3$. Spectroscopic studies of radicals obtained in the DMFIR of molecules show that the nascent radicals are characterized by a high vibrational excitation. Stephenson et al. [65] studied the energy partitioning in the CF_2 radicals generated in the collision-free multiphoton dissociation of CF_2HCl, CF_2Br_2 and CF_2Cl_2. The average vibrational energy of the CF_2 fragments was 3.6 kcal mol^{-1} for CF_2HCl, 1.8 kcal mol^{-1} for CF_2Br_2 and 2.9 kcal mol^{-1} for CF_2Cl_2. These values are consistent with vibrational Boltzmann distributions at 1160 K (CF_2HCl), 790 K (CF_2Br_2) and 1050 K (CF_2Cl_2). Thus, vibrational relaxation will produce a temperature increase that depends on the heat capacity of the buffer gas. Price and Ratajczak [66] studied the $Cl + NOCl \rightarrow Cl_2 + NO$, $Cl + SF_5Cl \rightarrow Cl_2 + SF_5$ and $Br + NOBr \rightarrow Br_2 + NO$ abstraction reactions at room temperature using a flash photolysis time of flight mass spectrometry system. They estimated that the temperature increases following the photolysis of NOCl, NOBr and SF_5Cl as the ratio of the excess energy liberated by the reaction to the total heat capacity of the gaseous system, and reported temperature increments of 750, 530 and 130 K, respectively. In a similar way, the temperature increment in our system can be estimated from the knowledge of the excess energy attained by $CDCl_3$ molecules in the DMFIR process. To our knowledge there are no previous works regarding the energy partitioning of CCl_2 radicals obtained by multiphoton dissociation of molecules reported in the literature. Although we have not determined the vibrational excitation attained by $CDCl_3$ molecules in the DMFIR process, we expect the samples would not be much heated in the experimental conditions of our work. This statement is made on one hand due to the high rate of dissociation of chloroform above the dissociation energy threshold. On the other hand, the experimental values of the rate constants reported have a weak pressure dependence consistent with the temperature range resulting from the fit.

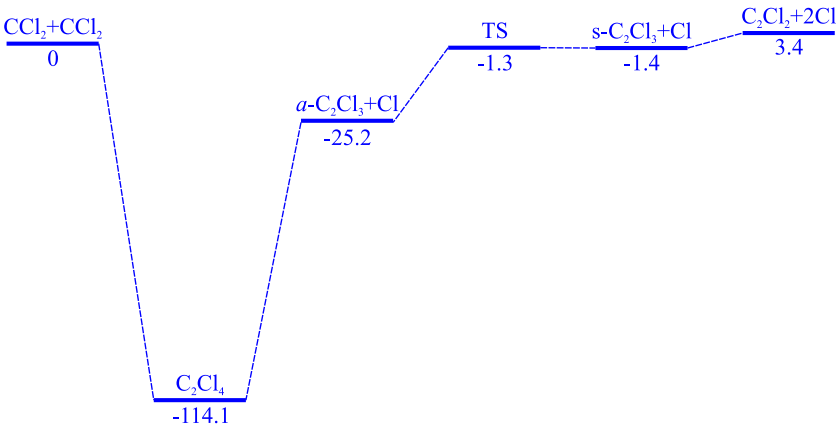

Fig. 9. Schematic energy diagram (in kcal mol^{-1}) for the self-recombination reaction of CCl_2 radicals. Calculations performed at the G4 level.

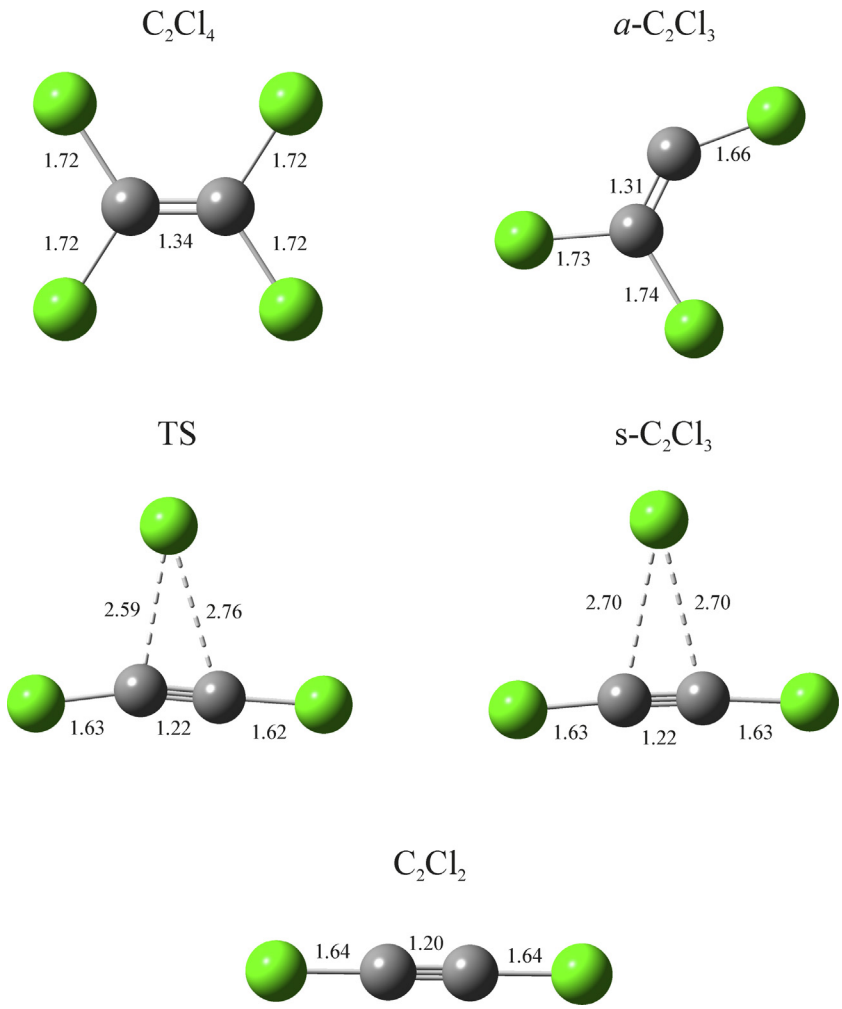

Fig. 10. Molecular geometries of the species depicted in the energy diagram showed in Fig. 9. Calculations correspond to the G4 model.

3.4. Reaction mechanism and discussion

Fig. 9 shows the schematic energy diagram for the $CCl_2 + CCl_2$ reaction based on G4 results. The geometries of the different species are depicted in Fig. 10.

The $CCl_2 + CCl_2$ reaction starts with the formation of a highly vibrationally excited complex $C_2Cl_4^*$. Afterwards, the reaction proceeds via its collisional stabilization to C_2Cl_4 or dissociation to $C_2Cl_3 + Cl$. In the absence of secondary reactions that deplete the concentration of the Cl and C_2Cl_3 species (by instance $Cl + Cl + M \rightarrow Cl_2 + M$ or the C_2Cl_3 self reaction which are expected to be slow), the fast reverse process $C_2Cl_3 + Cl \rightarrow C_2Cl_4$ ($k_\infty = 8.4 \times 10^{-10}$ cm^3 molecules^{-1} s^{-1} at 500 K, see Table S6.1 of Supplementary Material) completes the quantitative formation of C_2Cl_4. The participation of the Cl elimination channel $CCl_2 + CCl_2 \rightarrow C_2Cl_2 + 2Cl$ has been reported in high temperature experiments. This process was observed by Kumaran et al. in the thermal decomposition of $CHCl_3$ under varying density conditions and over the 1282–1878 K temperature range [2]. In that work, the C_2Cl_3 formation thorough reaction $CCl_2 + CCl_2 \rightarrow C_2Cl_3 + Cl$ followed by the very fast process $C_2Cl_3 \rightarrow C_2Cl_2 + Cl$ was proposed. This last process has been experimentally and theoretically studied by Bryukov et al. [67]. They found that Cl elimination proceeds via a transition state that connects the asymmetric (*a*) and symmetric (s) equilibrium configurations of the C_2Cl_3 radical (see Figs. 9 and 10). Further chemical transformation of the symmetric structure can be expected to favor dissociation via a very loose complex.

Reaction (1) was also considered as the main process in the mechanism postulated by Won and Bozzelli [1]. They studied the thermal decomposition of $CHCl_3$ diluted in Ar. QRRK calculations were performed to obtain the respective rate constants in high pressure conditions at 773–1273 K. The high pressure rate constant value of the i-C_3H_7 self-recombination reaction, 5.3×10^{-12} cm^3 molecule^{-1} s^{-1}, was used for that of the CCl_2 radicals self-recombination reaction. The results obtained with the SACM/CT and SSACM formalisms in the same temperature range are 1.2×10^{-12} cm^3 molecules^{-1} s^{-1} and 4.5×10^{-12} cm^3 molecules^{-1} s^{-1}, respectively. These results could explain the overestimation of the final concentration of C_2Cl_4 observed by Won and Bozzelli in their experiments.

4. Conclusions

In a previous work the kinetics of the $CCl_2 + CCl_2 \rightarrow C_2Cl_4$ association reaction has been experimentally studied [16]. The rate constant determined in the high pressure regime is $(6.7 \pm 0.2) \times 10^{-13}$ cm^3 molecule^{-1} s^{-1}. In the present study, the dependence of the rate constant over large temperature and the total pressure ranges was theoretically investigated. In the low pressure regime the rate constant calculated using Troe's factorized formalism is $k_0 = [Ar]\ 3.5 \times 10^{-23}\ (T/300\ K)^{-8.7} \exp(-1560\ K/T)$ cm^3 molecule^{-1} s^{-1}. The values calculated at the high pressure limit with the SSACM and SACM/CT formalisms are $k_\infty = (1.7 \pm 1.0) \times 10^{-12}$

$(T/300)^{0.8 \pm 0.1}$ cm^3 molecule^{-1} s^{-1} and $k_\infty = (5.4 \pm 3.0) \times 10^{-13}$ $(T/300)^{0.7 \pm 0.1}$ cm^3 molecule^{-1} s^{-1}, respectively. The experimental results of Ref. [16] for varying Ar pressure are consistent with the model values provided T is in the 500–700 K range, $-\langle\Delta E\rangle$ within 10 and 250 cm^{-1} and $k_\infty = 7.2 \times 10^{-13}$ cm^3 molecules^{-1} s^{-1}. This rate constant is consistent with those obtained with the SSACM and SACM/CT.

An analysis of the potential energy surface for the CCl_2 self-recombination reaction at the G4 level of theory showed that there is no barrier to recombination, and that the initially formed molecule has a vibrational excitation of ~114.1 kcal mol^{-1}. The energy of C_2Cl_3 + Cl is 25.2 kcal mol^{-1} below of the reactants. The C—Cl bond strength in C_2Cl_3 is 23.9 kcal mol^{-1}. The energy of C_2Cl_2 + 2Cl is about 3.4 kcal mol^{-1} higher than that corresponding to $2CCl_2$. Then, in the absence of secondary reactions of the Cl and C_2Cl_3 species, alternative to the C_2Cl_3 + Cl recombination, the CCl_2 recombination proceeds via the formation of C_2Cl_4 by collisional stabilization of the excited complex and by recombination of C_2Cl_3 with Cl.

Acknowledgements

This work was supported by the grants PIP 2010-0425 and PIP 2012-0134 from the Consejo Nacional de Investigaciones Científicas y Técnicas (CONICET) of Argentina and PICT-2012-0478 of the Agencia Nacional de Promoción Científica y Tecnológica.

Appendix A. Molecular parameters used in the modeling

Vibrational frequencies (cm^{-1}): C_2Cl_4: 288, 347, 1000, 176, 908, 512, 310, 777, 110, 237, 447, 1571. CCl_2: 730, 335.2, 757.9; CCl_2: 335, 730, 760 (from Ref. [68]).

Rotational constants (cm^{-1}): C_2Cl_4: 0.057, 0.046, 0.026. CCl_2: 1.67, 0.12, 0.11 (from B3LYP/MG3S calculations).

Dissociation energy, D_e: 117 kcal mol^{-1} (from G4 calculations).

Enthalpy of reaction at 0 K, $\Delta H^o_{R,0}$: 114 kcal mol^{-1} (from G4 calculations).

Lennard Jones parameters: $\sigma_{LJ}(C_2Cl_4)$ = 0.57 nm, σ_{LJ}(Ar) = 0.35 nm, $\varepsilon/k_B(C_2Cl_4)$ = 430 K, ε/k(Ar) = 114 K, (from Refs. [56,69]).

Appendix B. Supplementary material

Supplementary data include a video of the CCl_2 self-recombination. Calculated high pressure rate constants using the models SSACM and SACM/CT. Determination of the low pressure rate constant. Troe's formalism used to obtain the central broadening factor F_{cent} and its temperature dependence. Temperature dependence of the Kassel parameters (S_k and B_k). Determination of the rate constant for the Cl elimination reaction from C_2Cl_4, $C_2Cl_4 \rightarrow C_2Cl_3$+Cl. Supplementary data associated with this article can be found, in the online version, at https://doi.org/10.1016/j.comptc.2017.10.004. These data include MOL files and InChiKeys of the most important compounds described in this article.

References

[1] Y.S. Won, J.W. Bozzelli, Chloroform pyrolysis: experiment and detailed reaction model, Combust. Sci. Technol. 85 (1992) 345–373.
[2] S.S. Kumaran, M.C. Su, K.P. Lim, J.V. Michael, S. Klippenstein, J. DiFelice, P.S. Mudipalli, J.H. Kiefer, D.A. Dixon, K.A. Peterson, Experiments and theory on the thermal decomposition of $CHCl_3$ and the reactions of CCl_2, J. Phys. Chem. A 101 (1997) 8653–8661.
[3] P.H. Taylor, D. Lenoir, Chloroaromatic formation in incineration processes, Sci. Total Environ. 269 (2001) 1–24.
[4] G.P. Semeluk, R.B. Bernstein, The thermal decomposition of chloroform. I. products, J. Am. Chem. Soc. 76 (1954) 3793–3796.
[5] G.P. Semeluk, R.B. Bernstein, The thermal decomposition of chloroform. II. kinetics, J. Am. Chem. Soc. 79 (1957) 46–49.
[6] T. Yano, A shock tube study of the decomposition mechanism of chloroform in the presence of deuterium or methane, Bull. Chem. Soc. Jpn. 50 (1977) 1272–1277.
[7] I.P. Herman, F. Magnotta, R.J. Buss, Y.T. Lee, Infrared laser multiple-photon dissociation of $CDCl_3$ in a molecular beam, J. Chem. Phys. 79 (1983) 1789–1794.
[8] S.C. Chuang, J.W. Bozzelli, Conversion of chloroform to hydrochloric acid by reaction with hydrogen and water vapor, Environ. Sci. Technol. 20 (1986) 568–574.
[9] P.H. Taylor, B. Dellinger, Thermal degradation characteristics of chloromethane mixtures, Environ. Sci. Technol. 22 (1988) 438–447.
[10] P.H. Taylor, B. Dellinger, D.A. Tirey, Oxidative pyrolysis of CH_2Cl_2, $CHCl_3$, and CCl_4-I: incineration implications, Int. J. Chem. Kinet. 23 (1991) 1051–1074.
[11] G.P. Miller, V.A. Cundy, J.W. Bozzelli, The computational simulation of a stoichiometric CH_2Cl_2/CH_4/air flat flame, Combust. Sci. Technol. 98 (1994) 123–136.
[12] M. Kraft, E. Stöckelmann, H. Bockhorn, in: Twenty-Sixth Symposium (International) on Combustion, The Combustion Institute (1996) 2431–2437.
[13] Y.P. Wu, Y.S. Won, Pyrolysis of chloromethanes, Combust. Flame 122 (2000) 312–326.
[14] L. Zhu, J.W. Bozzelli, Kinetics and mechanism for the thermal chlorination of chloroform in the gas phase: inclusion of HCl elimination from $CHCl_3$, Int. J. Chem. Kinet. 35 (2003) 647–660.
[15] Y.S. Won, Thermal stability and reaction mechanism of chloromethanes in excess hydrogen atmosphere, J. Ind. Eng. Chem. 13 (2007) 400–405.
[16] N.D. Gómez, V. D'Accurso, F.A. Manzano, J. Codnia, M.L. Azcárate, Kinetic study of the CCl_2 radical recombination reaction by laser-induced fluorescence technique, Int. J. Chem. Kinet. 45 (2013) 306–313.
[17] N.D. Gómez, V. D'Accurso, F.A. Manzano, J. Codnia, M.L. Azcárate, Determination of the Rate Constant of the Reaction of CCl_2 with HCl, Int. J. Chem. Kinet. 46 (2014) 382–388.
[18] M.J. Frisch, et al., Gaussian 09. Revision D.01, Gaussian Inc., Wallingford, CT. 2009.
[19] S. Grimme, S. Ehrlich, L. Goerigk, Effect of the damping function in dispersion corrected density functional theory, J. Comp. Chem. 32 (2011) 1456–1465.
[20] A.D. Becke, Density-functional thermochemistry. III. The role of exact exchange, J. Chem. Phys. 98 (1993) 5648–5652.
[21] P.J. Wilson, T.J. Bradley, D.J. Tozer, Hybrid exchange-correlation functional determined from thermochemical data and ab initio potentials, J. Chem. Phys. 115 (2001) 9233–9242.
[22] H.L. Schmider, A.D. Becke, Optimized density functionals from the extended G2 test set, J. Chem. Phys. 108 (1998) 9624–9631.
[23] C. Adamo, V. Barone, Exchange functionals with improved long-range behavior and adiabatic connection methods without adjustable parameters: The mPW and mPW1PW models, J. Chem. Phys. 108 (1998) 664–675.
[24] J.M. Tao, J.P. Perdew, V.N. Staroverov, G.E. Scuseria, Climbing the density functional ladder: nonempirical meta-generalized gradient approximation designed for molecules and solids, Phys. Rev. Lett. 91 (2003) 146401 (1-4).
[25] J.P. Perdew, Electronic Structure of Solids 91, P. Ziesche, H. Eschrig(Eds.) , Akademie, Verlag, Berlin, 1991.
[26] J.P. Perdew, J.A. Chevary, S.H. Vosko, K.A. Jackson, M.R. Pederson, D.J. Singh, C. Fiolhais, Atoms, molecules, solids, and surfaces: applications of the generalized gradient approximation for exchange and correlation, Phys. Rev. B 46 (1992) 6671–6687.
[27] J.P. Perdew, J.A. Chevary, S.H. Vosko, K.A. Jackson, M.R. Pederson, D.J. Singh, C. Fiolhais, Erratum: atoms, molecules, solids, and surfaces - applications of the generalized gradient approximation for exchange and correlation, Phys. Rev. B 48 (1993) 4978.
[28] J.P. Perdew, K. Burke, Y. Wang, Generalized gradient approximation for the exchange-correlation hole of a many-electron system, Phys. Rev. B 54 (1996) 16533–16539.
[29] K. Burke, J.P. Perdew, Theory: Recent Progress and New Directions, J. F. Dobson, G. Vignale, M. P. Das(Eds.), Plenum, 1998.
[30] J.P. Perdew, Density-functional approximation for the correlation energy of the inhomogeneous electron gas, Phys. Rev. B 33 (1986) 8822–8824.
[31] A.D. Becke, Density-functional exchange-energy approximation with correct asymptotic-behavior, Phys. Rev. A 38 (1988) 3098–30100.
[32] C. Lee, W. Yang, R.G. Parr, Development of the Colle-Salvetti correlation-energy formula into a functional of the electron density, Phys. Rev. B 37 (1988) 785–789.
[33] B. Miehlich, A. Savin, H. Stoll, H. Preuss, Results obtained with the correlation-energy density functionals of Becke and Lee, Yang and Parr, Chem. Phys. Lett. 157 (1989) 200–206.
[34] J.P. Perdew, K. Burke, M. Ernzerhof, Generalized gradient approximation made simple, Phys. Rev. Lett. 77 (1996) 3865–3868.
[35] J.P. Perdew, K. Burke, M. Ernzerhof, Errata: generalized gradient approximation made simple, Phys. Rev. Lett. 78 (1997) 1396.
[36] X. Xu, W.A. Goddard III, The X3LYP extended density functional for accurate descriptions of nonbond interactions, spin states, and thermochemical properties, Proc. Natl. Acad. Sci. USA 101 (2004) 2673–2677.
[37] F.A. Hamprecht, A. Cohen, D.J. Tozer, N.C. Handy, Development and assessment of new exchange-correlation functionals, J. Chem. Phys. 109 (1998) 6264–6271.
[38] A. Austin, G. Petersson, M.J. Frisch, F.J. Dobek, G. Scalmani, K. Throssell, A density functional with spherical atom dispersion terms, J. Chem. Theory Comput. 8 (2012) 4989.

[39] Y. Tawada, T. Tsuneda, S. Yanagisawa, T. Yanai, K. Hirao, A long-range-corrected time-dependent density functional theory, J. Chem. Phys. 120 (2004) 8425–8433.
[40] O.A. Vydrov, G.E. Scuseria, Assessment of a long range corrected hybrid functional, J. Chem. Phys. 125 (2006) 234109.
[41] O.A. Vydrov, J. Heyd, A. Krukau, G.E. Scuseria, Importance of short-range versus long-range Hartree-Fock exchange for the performance of hybrid density functionals, J. Chem. Phys. 125 (2006) 074106.
[42] O.A. Vydrov, G.E. Scuseria, J.P. Perdew, Tests of functionals for systems with fractional electron number, J. Chem. Phys. 126 (2007) 154109.
[43] T. Yanai, D. Tew, N. Handy, A new hybrid exchange-correlation functional using the Coulomb-attenuating method (CAM-B3LYP), Chem. Phys. Lett. 393 (2004) 51–57.
[44] B.J. Lynch, Y. Zhao, D.G. Truhlar, Effectiveness of diffuse basis functions for calculating relative energies by density functional theory, J. Phys. Chem. A 107 (2003) 1384–1388.
[45] K.L. Schuchardt, B.T. Didier, T. Elsethagen, L. Sun, V. Gurumoorthi, J. Chase, J. Li, T.L. Windus, Basis set exchange: a community database for computational sciences, J. Chem. Inf. Model. 47 (2007) 1045–1052.
[46] J. Zheng, X. Xu, D.G. Truhlar, Minimal augmented Karlsruhe basis set, Theor. Chem. Acc. 128 (2011) 295–305.
[47] J. Troe, Theory of thermal unimolecular reactions at high pressures, J. Chem. Phys. 75 (1) (1981) 226–237.
[48] A.I. Maergoiz, E.E. Nikitin, J. Troe, V.G. Ushakov, Classical trajectory and statistical adibtic channel study of the dynamics of capture and unimolecular bond fission. V. Valence interactions between two linear rotors, J. Chem. Phys. 108 (4) (1998) 9987–9998.
[49] J. Troe, Theory of thermal unimolecular reactions at low pressures. II. Strong collision rate constants. Applications, J. of Chem. Phys 66 (1977) 4758–4775.
[50] J. Troe, Theory of thermal unimolecular reactions at low pressures I. Solutions of the master equation, J. Chem. Phys. 66 (1977) 4745–4757.
[51] J. Troe, Theory of thermal unimolecular reactions in the fall-off range. I. Strong collision rate constants, Ber. Bunsenges. Phys. Chem. 87 (1983) 161–169.
[52] J. Troe, V.G. Ushakov, Representation of broad fall-off curves for dissociation and recombination reactions, Z. Phys. Chem. 228 (2013) 1–10.
[53] C.J. Cobos, J. Troe, Theory of thermal unimolecular reactions at high pressures. II. Analysis of experimental results, J. Chem. Phys. 83 (3) (1985) 1010–1015.
[54] J.A. Montgomery, M.J. Frisch, J.W. Ochterski, G.A. Petersson, A complete basis set model chemistry. VI. Use of the density functional geometries and frequencies, J. Chem. Phys. 110 (1999) 2822.
[55] L.A. Curtiss P.C. Redfern, Krishnan Raghavachari, Gaussian 4 Theory, J. Chem. Phys. 126 2007 084108–84111.
[56] C.J. Cobos, A.E. Croce, K. Luther, L. Solter, E. Tellbach, J. Troe, Experimental and modeling study of the reaction $C_2F_4(+M) \leftrightarrow CF_2 + CF_2(+M)$, J. Phys. Chem. A 117 (2013) 11420–11429.
[57] I. Oref, D.C. Tardy, Energy transfer in highly excited large polyatomic molecules, Chem. Rev. 90 (1990) 1407–1445.
[58] NIST- JANAF thermochemistry database. <http://kinetics.nist.gov/janaf/janaf4pdf.html>.
[59] A. Burcat, B. Ruscic, Third Millenium Ideal Gas and Condensed Phase Thermochemical Database for Combustion with Updates from Active Thermochemical Tables, 2015.
[60] J. Demaison, L. Margules, J.M.L. Martin, E. Boggs, Anharmonic force field, structure, and thermochemistry of CF_2 and CCl_2, Phys. Chem. Chem. Phys. 4 (2002) 3282–3288.
[61] K. Sendt, G.B. Bacskay, Spectroscopy constants of the X~($^1A_1$), ã($^3B_1$) and $\tilde{A}(^1B_1)$ states of CF_2, CCl_2 and CBr 2 and heats of formation of selected halocarbenes: an ab initio quantum chemical study, J. Chem. Phys. 112 (2000) 2227–2238.
[62] J. Troe, V.G. Ushakov, Revisiting falloff curves of thermal unimolecular reactions, J. Chem. Phys. 135 (2011) 054304–54311.
[63] H. Hippler, J. Troe, Ricent direct studies of collisional energy transfer in vibrationally highly excited molecules in the ground electronic State. Bimolecular collisions, J.E. Baggott, M.N. Ashfold(Eds.), The Royal Society of Chemistry, London, 1989.
[64] G.W. Flynn, Collision-induced eenrgy flow between vibrational modes of smll polyatomic molecules, Acc. Chem. Res. 14 (1981) 334–341.
[65] J.C. Stephenson, D.S. King, Energy partitioning in the collisionfree multiphoton dissociation of molecules: energy of CF_2 from CF_2HCl, CF_2Br 2 and C_F2C_l2, J. Chem. Phys. 69 (1978) 1485–1492.
[66] D. Price, E. Ratajczak, Kinetic studies using photolysis time of flight mass spectrometry system: determination of the rate constants for the abstraction reactions Cl + NOCl, Cl + SF_5Cl and Br + NOBr, Bull. de L'Academie Polonaise des Sci. 27 (3) (1979) 195.
[67] M.G. Bryukov, S.A. Kostina, V.D. Knyazev, Kinetics of the unimolecular decomposition of the C_2Cl_3 radical, J. Phys. Chem. A 107 (2003) 6574–6579.
[68] <http://webbook.nist.gov/chemistry>.
[69] R.C. Reid, J.M. Prausnitz, B.E. Poling, The Properties of Gases and Liquids, fourth Ed., McGraw-Hill, New York, United States, 1987.